Nuclear Polarization of Short-lived Na Isotopes Maintained in Single Crystals for β-NMR Spectroscopy

K. Minamisono[a,b,1], K. Matsuta[c], T. Minamisono[c,2], C. D. P. Levy[a], T. Nagatomo[c,3], M. Ogura[c], T. Sumikama[c,4], J. A. Behr[a], K. P. Jackson[a], M. Mihara[c], M. Fukuda[c]

[a] *TRIUMF, 4004 Wesbrook Mall, Vancouver, BC V6T 2A3, Canada*
[b] *National Superconducting Cyclotron Laboratory, Michigan State University, East Lansing, MI 48824 USA*
[c] *Department of Physics, Osaka University, Toyonaka 560-0043, Osaka Japan*

Abstract

A compact β-ray detecting nuclear magnetic/quadrupole resonance system with a permanent magnet was developed at ISAC/TRIUMF to measure ground-state electromagnetic moments of short-lived nuclei. Polarized Na beams produced using the collinear optical-pumping technique were used to demonstrate the properties of the system. The degree of nuclear polarization and the spin-lattice relaxation times of the ^{20,21,26,27,28}Na isotopes in NaF, TiO_2, $LiNbO_3$, MgF_2, ZnO, Pt, and Mg single crystals at room temperature are reported. The electric-quadrupole coupling constants of ^{20,21}Na in TiO_2, ZnO and Mg, and that of ^{27}Na in ZnO are also reported. The quadrupole moments of ^{20,21}Na were extracted from the electric-quadrupole coupling constants in ZnO, using the known quadrupole moment of ^{27}Na.

Keywords: nuclear polarization, optical pumping, β NMR, nuclear-spin lattice relaxation time, electromagnetic nuclear moment

Email address: minamiso@nscl.msu.edu (K. Minamisono)

[1] Japan Society for the Promotion of Science, Postdoctoral Fellowships for Research Abroad

[2] Present address: Department for the Application of Nuclear Technology, Fukui University of Technology, Gakuen, Fukui 910-8505, Japan

[3] Present address: Department of Chemistry, International Christian University, Mitaka, Tokyo 181-8585, Japan

[4] Present address: Department of Physics, Tokyo University of Science, Noda, Chiba 278-8510, Japan

PACS: 21.10.Ky, 27.30.+t, 29.27.Hj, 76.60.-k, 76.60.Gv

1. INTRODUCTION

Recent developments in the production of radioactive nuclear beams have made it possible to perform studies of nuclear moments [1, 2] away from the line of β stability in the nuclear chart, and have expanded possibilities for materials studies with short-lived probes [3]. Good quality (low emittance) and intense radioactive beams are provided at isotope online separator (ISOL) facilities. Laser spectroscopy, which demands such beam properties, has been widely used to determine nuclear properties [4] such as spin (I), magnetic-dipole moment (μ), electric-quadrupole moment (Q), and mean-square charge radius, $\langle r^2 \rangle$. These are fundamental properties of a nucleus and provide key information on nuclear structure. The μ and Q interact with external and internal fields through the well-known electromagnetic interactions and are readily used to test various theories which attempt to reproduce experimental data.

Optical-pumping techniques have also been successfully applied to beams obtained at ISOL facilities to produce nuclear polarization. These polarized beams, combined with a subsequent β-ray detecting nuclear magnetic resonance (β-NMR) technique [5, 6], can be used to determine precise values of μ and Q for the beam nuclei, and to study materials with high sensitivity. The β-NMR signal is obtained by detecting the asymmetric β-ray angular distribution from the decaying polarized nuclei, and typically requires a source strength of order 10^3 decays/second. Although β NMR is limited to nuclei with relatively short half-lives ($T_{1/2} \sim$ a few seconds or less) due to the relaxation time of polarization, the β-NMR technique is more sensitive than standard fluorescence detection in laser spectroscopy, which can suffer from high background. β NMR is especially favored for measurements in which the hyperfine structure becomes difficult to resolve, for example Q measurements in light elements [6, 7]. Therefore, μ and Q measurements, particularly away from the valley of stability, are best performed by β NMR.

One key to a successful β-NMR measurement is a large nuclear polarization, as the figure of merit (YP^2, where Y and P are counting rate and polarization, respectively) for such a measurement is proportional to the magnitude of polarization squared. Typical polarizations achieved through

optical pumping are larger than 40% for alkali elements [8, 9], making measurements more reliable and efficient due to the high YP^2, than those with low YP^2. With the advances in laser technology, and the development of new optical pumping techniques, for example pumping from meta stable states [10, 11] with existing lasers, optical pumping, and thus β-NMR can be applied to a large and increasing number of isotopes. Nuclear reaction techniques are also used to produce polarization [12, 13], but the polarization produced is typically a few percent. Reversing the polarity of nuclear polarization is also rather difficult in the nuclear reaction technique, whereas in the optical-pumping technique, switching between polarities can be easily achieved by changing the helicity of the laser light. Some potential systematic errors, due to multiple radio frequency application, in the measurement of Q with the β-NMR technique are removed by measuring two separate NMR spectra with opposite laser helicities. An overview of the production of spin-oriented beams is given in Ref. [14].

Another important component of a successful β-NMR measurement is the choice of the implantation crystal. The crystal host provides an electric field gradient that can probe Q, as well as a symmetric lattice to maintain the polarization of the implanted nucleus. The final location of the implanted nucleus may be a substitutional and/or an interstitial site of the crystal lattice with a long polarization relaxation time, depending on the temperature. However, it is often difficult to find crystals that provide such an environment and an electric field gradient appropriate for β-NMR measurements. Preliminary studies are usually required for a specific combination of a crystal and implanted nucleus. Such basic knowledge is indispensable for the reliable and precise determination of electromagnetic moments. Once information is obtained for a given element it can provide the basis for a choice of crystal for other nuclei in the same group of the periodic table as the nucleus studied, and even for nearby elements, if the chemical properties are similar.

A compact β-ray detecting nuclear magnetic/quadrupole resonance system with a permanent magnet was constructed at ISAC/TRIUMF to measure the ground-state electromagnetic moments of radioactive nuclides. Highly polarized ^{20,21,26,27,28}Na beams were produced by a collinear-laser pumping technique. The nuclear polarization maintained in NaF, TiO_2, $LiNbO_3$, MgF_2, ZnO, Pt and Mg single crystals, and the spin-lattice relaxation times for all five Na beams (except the relaxation time of ^{28}Na) were studied. The electric-quadrupole coupling constants of ^{20,21}Na in TiO_2, ZnO and Mg single crystals were also investigated. The preliminary results were reported in Ref.

[15]. Based on the knowledge obtained, new values of Q for the ^{20}Na and ^{21}Na ground states could be determined [16]. The present paper provides a detailed description of the β-NMR system developed at ISAC/TRIUMF.

2. EXPERIMENT

2.1. Production and Measurement of Polarization

The experiments were performed at the radioactive nuclear beam facility ISAC-I at TRIUMF. The measurements of ^{20,21,26,27,28}Na were performed in separate runs. The experimental procedure in the measurement of ^{20}Na is explained below. Similar procedures were used in the measurements of the other Na isotopes.

The 500 MeV proton beam from the TRIUMF cyclotron was used to bombard a thick SiC production target (a Ta target was used for the production of ^{28}Na), which was coupled to a surface ion source. ^{20}Na singly-charged ions were extracted at an energy of 40.8 keV and mass separated. The pure ^{20}Na beam was transported to the polarizer beam line [17], which is shown schematically in Fig. 1, in the ISAC-I experimental hall. The ion beam was first passed through a Na-vapor cell and partially neutralized by charge exchange. After neutralization, Na atoms were polarized using collinear optical pumping on the 589.8 nm (vacuum) D_1 transition ($3s\ 2S_{1/2} \leftrightarrow 3p\ 2P_{1/2}$), with circularly polarized light [5]. The remaining ion component of the exiting beam from the Na cell was removed by an electrostatic deflector, as the ionic component was unpolarized and reduced the resulting polarization. The velocity of the ^{20}Na beam was adjusted to tune the Doppler-shifted laser frequency into resonance with the D_1 transition, by applying a bias voltage to the accelerating/decelerating electrodes at the entrance to the Na-vapor cell. Both of the ground state hyperfine levels ($3s\ 2S_{1/2}\ F = I + 1/2$ and $I - 1/2$) were pumped to achieve high polarization using side band frequencies produced by an electro-optic modulator (EOM), a technique that was successfully employed in the past [18]. The collinear laser light was generated by a frequency-stabilized ring-dye-laser (Coherent 899-21) pumped by a 7-W argon-ion laser. After passing through a 1.9 m interaction region with the laser light, the polarized ^{20}Na beam was re-ionized in a differentially-pumped He-gas target.

Polarization loss in the re-ionization process may occur due to a multiple collision ionization and/or an inner ($1s$) electron removal processes. However, the main ionization process is assumed to be a direct ionization (removal of

the $2s$ electron), which occurs in too short of a time period to affect the nuclear polarization. Since ∼80% polarization for ^{8}Li was produced with the same technique [18], the upper limit of the polarization loss due to the re-ionization process is expected to be ∼20%. The main polarization loss is due to the mismatch of the laser line widths to the atomic absorption line. Due to the multiple scattering with Na vapor atoms in the neutralization process, the line width was typically 100 MHz, much wider than the natural line width.

The polarized ^{20}Na ions were transported to the β-NMR apparatus, which is illustrated in Fig. 2, and implanted into a single crystal. The crystal was typically 10 mm × 10 mm and 0.5 mm in thickness. For the NaF crystal, a large NaF single crystal was cleaved just before installation in the vacuum chamber, and the fresh surface was used for implantation. The surface of the Mg single crystal was etched by a few micrometer just before the measurement using a ∼3 % solution of citric acid. A Pt foil of ∼10 μm in thickness was annealed at ∼1000 °C for ∼10 hours to remove local stress in the foil prior to the measurement. The surfaces of all other crystals were polished by manufactures. Typical implantation depth of the 40.8 keV ^{20}Na beam into NaF crystal was ∼ 500Å.

An external magnetic field was produced by a permanent magnet ($Nd_2Fe_{14}B$) and applied parallel to the direction of polarization, to maintain the polarization in the crystal. The NMR magnet (permanent magnets and a return yoke made of iron) are shown in Fig. 3. A pair of permanent-magnet poles was attached to the return yoke. The permanent magnet consisted of eight pieces of permanent magnet, which were glued together, as schematically illustrated in Fig. 4. The direction of the magnetization axis of each of the magnet segments was adjusted to 56° relative to the normal of the pole face to generate a strong and uniform magnetic field at the center of the magnet as shown in Figs. 4 and 5. The angle was determined by field calculations with a code PANDIRA [19]. The central magnetic field, measured by a Hall probe, was $H_0 = 0.5286$ T. The result of calculation was about 2% larger than the measured value, which was attributed to the accuracy of parameters used for the permanent magnet material in the calculation. A sufficient field uniformity of ∼ 0.1% relative to the central magnetic field was achieved within the 5 mm diameter implantation area of the Na beam, as shown in Fig. 6. The calculated relative field uniformity is also plotted in the figure. The difference between calculations and measurements is due to a simplified geometry of the NMR magnet in the calculation.

The ^{20}Na nucleus undergoes β decay, with a half-life of 447.9 ms, mainly populating the first excited state in the daughter nucleus, ^{20}Ne. The maximum β-ray energy for the decay is 11.23 MeV. The β rays were detected by the coincidence between large-plastic scintillator (counter E; 160 mm in diameter and 120 mm long) and two thin plastic scintillators [see Fig. 2]. One of the thin plastic scintillators was placed near the implantation crystal (counter A; 12 mm in diameter and 0.5 mm thick), while the other was placed right before the counter E (counter B; 55 mm in diameter and 1 mm thick), defining the solid angle of the detector system. A cone-shaped air-core plastic scintillator (counter C) was placed in the magnet to veto β rays that scattered from the surface of the magnet. All of the β detectors were placed outside the vacuum chamber, and β rays passed through a thin plastic vacuum window (0.1 mm thick) before reaching the detectors. The two detector telescopes were placed at 0°(u) and 180°(d) relative to the direction of polarization.

The counting rate is asymmetric between the u and d counters for a polarized source. The angular distribution of β rays,

$$W(\varphi) \sim 1 + AP\cos\varphi, \tag{1}$$

depends on the asymmetry parameter A (+1/3, for ^{20}Na β decay to the first excited state in ^{20}Ne), the polarization P and the angle φ between the direction of momentum of the decay β ray and the polarization axis. The degree of polarization maintained in the implantation crystal can be obtained from an asymmetry change, AP, in the β-decay angular distribution:

$$AP = \frac{\sqrt{R}-1}{\sqrt{R}+1}. \tag{2}$$

The double ratio, R, is defined by β-ray counts, $W(\varphi)$, as

$$R = \left[\frac{W(0^\circ)}{W(180^\circ)}\right]_+ \Bigg/ \left[\frac{W(0^\circ)}{W(180^\circ)}\right]_-, \tag{3}$$

which compensates for different detector efficiencies. In Eq. (3) the subscript, + (−), stands for the ratio measured with positive- (negative-) helicity laser light. The polarization changes sign ($P \to -P$) depending on the helicity of the laser light as the maximum (minimum) nuclear magnetic-quantum number is heavily populated by the positive- (negative-) helicity laser light.

The spin-lattice relaxation time, T_1, of the polarization in a given implantation crystal can also be extracted from a measurement of the time dependent variation in the value of AP. A pulsed beam method was employed using a fast electrostatic kicker. A 500-ms implantation time was followed by a 1-s β-ray counting time. The sequence, or the timing program, was repeated until sufficient statistics were achieved.

2.2. Electromagnetic Interaction

The Hamiltonian of the electromagnetic interaction between nuclear moments and external fields [20] is given by

$$H = -\boldsymbol{\mu} \cdot \boldsymbol{H}_0 + \frac{eqQ}{4I(2I-1)}\{3I_Z^2 - I(I+1) + \frac{\eta}{2}(I_+^2 + I_-^2)\}, \qquad (4)$$

where $\boldsymbol{\mu}$ is the magnetic moment, $\boldsymbol{H}_0$ is the external magnetic field, I_z is the third component of the spin operator and $I_\pm$ are the spin raising and lowering operators. The largest component of the electric field gradient is defined by $q = V_{ZZ}$ where V is the electrostatic potential and $V_{ii} = d^2V/di^2$ with $V_{XX} + V_{YY} + V_{ZZ} = 0$. The asymmetry parameter of the electric field gradient is defined as $\eta = (V_{XX} - V_{YY})/V_{ZZ}$, with $|V_{XX}| \leq |V_{YY}| \leq |V_{ZZ}|$. An electric field gradient is provided by the internal field of a single crystal. The energy levels are given by

$$E_m = -g\mu_N H_0 m + \frac{h\nu_Q}{12}(3\cos^2\theta - 1 + \eta\sin^2\theta\cos 2\phi)\{3m^2 - I(I+1)\}, \quad (5)$$

where, for simplicity, the electric-quadrupole interaction is regarded as a perturbation to the main magnetic-dipole interaction and Eq. (5) is given to first-order of the electric-quadrupole coupling constant, eqQ/h, with $\nu_Q = 3eqQ/\{2I(2I-1)h\}$ being a normalized electric-quadrupole coupling frequency. In Eq. (5), m is the magnetic quantum number, and θ and ϕ are the Euler angles between the principal axes of the electric field gradient and H_0, respectively. The first term in Eq. (5) gives the $2I+1$ magnetic substates separated by a fixed energy value, determined from the applied H_0 and the nuclear g factor, due to the magnetic-dipole interaction (Zeeman splitting). These substates are further shifted by the electric-quadrupole interaction and the energy spacing between adjacent substates is no longer constant. The $2I$ separate transition frequencies appear as

$$\nu_{m-1\leftrightarrow m} = \nu_L - \frac{\nu_Q}{4}(3\cos^2\theta - 1 + \eta\sin^2\theta\cos 2\phi)(2m-1), \qquad (6)$$

since the transition frequencies correspond to the energy difference between two adjacent energy levels ($\Delta m = \pm 1$) in Eq. (5). Here $\nu_L = g\mu_N H_0/h$ is the Larmor frequency. The variation in the number and position of resonance frequencies between the pure magnetic-dipole interaction and both the magnetic-dipole and electric-quadrupole interactions is schematically shown in Fig. 7 for the case of $I = 2$. It is noted that when the electric-quadrupole interaction cannot be considered as a perturbation to the magnetic-dipole interaction, higher-order terms of the electric-quadrupole interaction have to be considered. Higher-order terms were considered in the measurements of eqQ/h of ^{20,21}Na in TiO_2 and ^{20}Na in ZnO, due to the condition of $\nu_L \sim \nu_Q$. For the other eqQ/h measurements, the perturbation technique may be applied because the condition of $\nu_L \gg \nu_Q$ was fulfilled for the relevant region of eqQ/h.

2.3. β-NMR/NQR system

The β-NMR technique can be applied to such a system, where the nucleus interacts with external electromagnetic fields. An NMR signal is obtained using the double ratio given in Eq. (3), where, in this case, the subscript $+$ $(-)$ stands for a ratio with (without) the application of the radio frequency (RF) field. An adiabatic-fast passage (AFP) method [21] was used in the RF application. AFP provides an efficient NMR measurement, as it leads to an inversion of the initial polarization ($P \rightarrow -P$) produced by the optical-pumping technique, effectively doubling the signal as compared to the more traditional depolarization method.

The electric-quadrupole interaction is most efficiently probed by NMR when all of the $2I$ transition frequencies in Eq. (6) are applied in a time period that is short compared with the lifetime of the nucleus. This procedure ensures saturation of all transitions in Eq. (6) at eqQ/h on resonance. For example, the signal obtained for a nucleus with $I = 2$ (as in the case of ^{20}Na) in the AFP method with multiple-transition frequencies is 20 times larger than that obtained by applying a single-transition frequency, where only a partial saturation of transitions can be achieved. In this comparison, a linear distribution of populations in E_m is assumed as $a_m - a_{m-1} = \epsilon$ and $\sum_{m=-I}^{I} a_m = 1$, where a_m is the substate population, with magnetic quantum number m, and ϵ is a constant. This multiple frequency version of the β-NMR technique is known as the β-ray detecting nuclear-quadrupole resonance (β NQR) technique [22] and is discussed in detail elsewhere [23].

A schematic of the β-NQR system is shown in Fig. 8. A computer-controlled RF generating system produced an RF signal, which was sent to a 300-W amplifier. The amplified signal was applied to an RF coil, which was part of a LC resonance circuit. The circuit included an impedance matching transformer and a bank of six selectable variable capacitors. After applying the first frequency to ^{20}Na for 10 ms, another frequency was generated by the RF generating system and sent to the same LC resonance circuit. A different capacitor, which was tuned to satisfy the LC resonance condition for the second frequency, was selected by the fast-switching relay system. The system ensured sufficient power (the oscillating magnetic field strength, $H_1 \sim 1$ mT) for any set of four transition frequencies for ^{20}Na over the expected search region of eqQ/h. The switching time between RF signals was 3 ms.

The AFP interchanged the a_{m-1} and a_m populations when the RF corresponded to the transition frequency between adjacent $m-1$ and m substates. The total inversion of polarization ($P \rightarrow -P$) was achieved by applying RF sequentially, as illustrated for ^{20}Na in Fig. 9. In Fig. 9, $1 \leftrightarrow 2$ corresponds to an application of the transition frequency between the $m = 1$ and 2 magnetic substates, and the populations in these two substates are interchanged by the AFP. After 10 sequential applications of transition frequencies, the direction of initial polarization is inverted, where P is defined by $P = \sum_{m=-I}^{I} a_m m/I$. The inversion efficiency, α, defined by $P_1 = \alpha P$ with P_1 being the inverted polarization, was determined in three separate measurements. Up-down β-ray counting ratios were measured for non-inverted polarization (R), inverted polarization (R_1) and twice inverted polarization (R_2). The twice inverted polarization was achieved with 20 sequential applications of transition frequencies and the direction of polarization pointed the same direction as the initial polarization. These ratios are given by

$$R = g\frac{1+AP}{1-AP}, \quad R_1 = g\frac{1+\alpha AP}{1-\alpha AP}, \quad R_2 = g\frac{1+\alpha^2 AP}{1-\alpha^2 AP}. \tag{7}$$

Here g is a geometrical factor due mainly to a small difference in the solid angles and efficiency of the up and down detectors. The α can be extracted by solving Eq. (7) for α, g and AP. Typically, $\alpha \sim -0.81$ was achieved. Each applied RF was swept only once in the RF time of 10 ms from one frequency to another with a width of FM = $\pm$ 20 kHz. The FM was also used to cover a certain region of eqQ/h for an effective search of the resonance. An amplitude modulation was also applied to the RF for an efficient AFP. At the beginning and end of the FM sweep, the H_1 was reduced to ~ 0.02 mT and

gradually increased to the maximum $H_1 \sim 0.8$ mT to avoid depolarization due to the sudden start and stop of the strong H_1. The pulsed beam method was employed. A 500-ms implantation time was followed by the RF time and then by a 1-s β-ray counting time. The timing program was repeated until the required statistics were achieved.

3. RESULT AND DISCUSSION

3.1. Production and Measurement of Polarization

All measurements were performed at room temperature (RT). A typical result of the polarization measurement of ^{20}Na in a NaF single crystal is shown in Fig. 10. The upper plot in the figure depicts the u/d β-ray counting ratio as a function of the bias voltage at the Na neutralizer (equivalent to the laser frequency) [see Fig. 1]. The solid circles were measured with positive-helicity and the open circles with negative-helicity laser light. The value of AP, extracted using Eq. (2), is plotted in the lower portion of the figure. The maximum value of AP was about 16%, obtained at a bias voltage of $\sim$100 V. The polarization results are summarized in Table 1, which includes results of polarization in other single crystals (TiO_2, $LiNbO_3$, MgF_2, ZnO, Pt and Mg) and for the other Na isotopes.

The value of AP is a measure of the polarization averaged over the β-ray counting time over many cycles of the timing program. The time-dependent variation of AP was measured for ^{20}Na implanted in several crystals, and results are presented in Fig. 11. The value of T_1 are extracted from fits of an exponential function to the relaxation curves and the results are summarized in Table 1. The initial polarization, P_0, is extracted in each case from the AP by correcting for the A and T_1 considering $T_{1/2}$ and the timing program used. The values of A, determined by integrating over the measured β-decay branches, and used in extraction of P_0 are also included in Table 1.

The P_0s of a given Na isotope in different crystals vary in magnitude. This may be attributed to a very fast depolarization due to the roughness and cleanliness of the surface of the crystal and/or a depolarization effect in the process of implantation.

The NaF crystal has values of T_1 that are long compared to the nuclear lifetime for all Na isotopes except ^{21}Na, which has a long $T_{1/2} = 22.49$ s. This result is attributed to the occupation of implanted Na ions in substitutional sites in the NaF crystal, where a symmetric environment is provided. A T_1 in an ionic crystal is known to be dominated by quadrupole interaction

[25, 26] and the quadrupolar T_1 is given by $T_1 \propto Q^{-2}$. The T_1s of ^{26}Na (which has the smallest Q in the preset study) in ionic crystals are longer than those of ^{20,21}Na isotopes [see Table I], which have large Q. However, ratios of T_1 of those nuclei are not scaled by Q^{-2}. It is also noted that the T_1s of ^{27}Na (which has a small but 35 % larger Q than that of ^{26}Na) in ionic crystals are almost the same as those of ^{20,21}Na. These inconsistencies with Q^{-2} dependence of T_1 may be attributed to the roughness and/or different conditions of the crystal surfaces in each measurement.

Pt maintains the polarization of ^{20}Na well, with a long T_1, but ^{26}Na in Pt has very short T_1 and the AP is small. The large difference for the T_1 between ^{20}Na and ^{26}Na in Pt may be explained by the difference in gyromagnetic ratios ($\gamma = g\mu_N/\hbar$). The T_1 of a nucleus implanted in a metal is mainly determined by the Fermi contact interaction between the magnetic moments of the conduction electron in the s orbit and the nucleus. The Korringa relation is introduced for T_1 in metal [27]:

$$T_1 T K^2 = \frac{h}{8\pi^2 k_B} \left(\frac{\gamma_e}{\gamma_N} \right)^2 , \tag{8}$$

where T is the temperature, K is the Knight shift, k_B is the Boltzmann constant, and the subscripts e and N represent the electron and nucleus, respectively. The T_1 between two isotopes can be related at the same T as:

$$\frac{T_1^{(1)}}{T_1^{(2)}} = \left(\frac{\gamma_N^{(2)}}{\gamma_N^{(1)}} \right)^2 . \tag{9}$$

The present result of the ratio, $T_1^{(20)}/T_1^{(26)} = 28 \pm 4$, between ^{20}Na and ^{26}Na is consistent with the known ratio of γ_N, $(\gamma_N^{(26)}/\gamma_N^{(20)})^2 = 26.47 \pm 0.05$ [24], and satisfies the relation given in Eq. (9). This result supports the dominance of the Fermi-contact interaction in the T_1 of Na isotopes in Pt.

3.2. Magnetic Moment of ^{20}Na

The β-NMR/NQR system was used to measure Q of ^{20,21}Na [16]. The measurement of the known magnetic moment of ^{20}Na, where no electric-quadrupole interaction is required, was needed to determine the ν_L before the Q measurement. Precise determination of ν_L is important, since the expected transition frequencies of ^{20}Na in the presence of an electric-quadrupole

interaction are given relative to ν_L, as shown in Eq. (6) and Fig. 7. The polarized ^{20}Na ions were implanted into a cubic NaF single crystal placed at the center of the NMR magnet, where the β-NMR technique was applied. One of the relays in the β-NQR system shown in Fig. 8 was kept closed and the system worked as a single LC resonance circuit, since only a single-transition frequency is required to search for the NMR condition. A depolarization method was used to precisely determine the ν_L, because AFP requires higher RF power to saturate a transition and, as a result, tends to broaden the line width of the resonance. RF was applied with a FM = $\pm$ 2 kHz and without AM. The FM was swept $\sim$ 8 times within the RF time of 100 ms. The applied H_1 was $\sim$ 0.3 mT. The resulting NMR spectrum is shown in Fig. 12. The data point taken at 9000 kHz determines the baseline. A Gaussian was used to fit the resonance and the obtained centroid was 744.5 $\pm$ 0.1(stat.) $\pm$ 0.3(syst.) kHz. A contribution of 10% of the line width was added as a systematic error [28]. The μ was deduced, using the external magnetic field of $H_0 = 0.5286 \pm 0.0005$ T and $I = 2$, to be $|\mu(^{20}\mathrm{Na})| = 0.3694 \pm 0.0001$(stat.) $\pm$ 0.0004(syst.) μ_N, where the uncertainty of H_0 was added to the systematic error. The chemical shift of Na in NaF [29] was not considered since the shift is smaller than the error in the result. The present result agrees with the previous value, $\mu(^{20}\mathrm{Na}) = +0.3694 \pm 0.0002\ \mu_\mathrm{N}$ [30].

3.3. Electric-Quadrupole Coupling Constants of ^{20}Na and ^{21}Na

The eqQ/h of ^{20}Na was determined in Mg, but the measurement of eqQ/h was not performed for other Na isotopes since shorter T_1s are expected at the room temperature due to the Fermi contact interaction in a metal, as discussed above for Pt. The eqQ/h of ^{21}Na was determined in TiO_2, but no meaningful spectrum was obtained for ^{20}Na due to unknown causes. The η of TiO_2 was determined by measuring β-NQR spectra of ^{21}Na both with the c-axis parallel and perpendicular to B_0. All the results are summarized in Table 1.

The eqQ/h of both ^{20}Na and ^{21}Na were determined in ZnO. The q of ZnO is parallel to the c-axis with $\eta = 0$ due to the crystal structure. The c-axis was set perpendicular to the external-magnetic field ($\theta = 90^\circ$). The electric-quadrupole coupling constant of ^{20}Na in ZnO was searched for by varying four transition frequencies for a given trial eqQ/h. The transition frequencies were obtained by numerically solving the Hamiltonian given in Eq. (4), since the electric-quadrupole interaction can not be considered as a perturbation to the magnetic-dipole interaction, due to the condition of $\nu_Q \sim \nu_L$. RFs were

sequentially applied for AFP as explained above and in Fig. 9. FM of ±20 kHz and AM were applied. The β-NQR spectrum of ^{20}Na and ^{21}Na in ZnO is shown in Fig. 13, where $2AP_{av}$ is plotted as a function of trial eqQ/h. The $2AP_{av}$ is the difference between AP measured with positive-helicity (σ^+) and negative-helicity (σ^-) laser light, $2AP_{av} \equiv AP(\sigma^+) - AP(\sigma^-)$. Two separate measurements of NMR spectra with opposite helicity laser lights remove possible ambiguities due to multiple RF application, in determining the centroid, and maximize the NMR signal for an accurate measurement. The solid circles in Fig. 13 are the experimental data and the horizontal bar on each point is the range of eqQ/h covered by the FM.

There appear to be two final Na ion sites in ZnO, where the crystal lattice exerts different q. A two component Gaussian best fit to the data is shown in the solid line. The measurement of the resonance at low eqQ/h of ^{20}Na in ZnO was incomplete as seen in Fig. 13, as no data points were taken below $eqQ/h \sim 200$ kHz. Therefore, the ratios of the centroids (namely the ratio of electric field gradients), the amplitudes and the line widths between the two resonances were taken from the fit of ^{21}Na in ZnO. The fit results give eqQ/h of ^{20,21}Na in ZnO at the dominant site as

$$\left|\frac{eqQ(^{20}\mathrm{Na})}{h}\right|_{\mathrm{ZnO}} = 690 \pm 12 \ \ \mathrm{kHz}, \tag{10}$$

$$\left|\frac{eqQ(^{21}\mathrm{Na})}{h}\right|_{\mathrm{ZnO}} = 939 \pm 14 \ \ \mathrm{kHz}. \tag{11}$$

The error contains the systematic error in determining the centroid caused by possible variations of the centroid of the resonance at low eqQ/h.

The eqQ/h of ^{27}Na in ZnO was also measured since the Q is precisely known from a separate measurement, $Q(^{27}\mathrm{Na}) = 0.72 \pm 0.03$ e fm^2 [8], and can serve as a reference to extract $Q(^{20}\mathrm{Na})$ and $Q(^{21}\mathrm{Na})$. The β-NQR spectrum of ^{27}Na in ZnO is shown in Fig. 13. Since the eqQ/h is small due to the small $Q(^{27}\mathrm{Na})$, the c-axis was set parallel to the external magnetic field ($\theta = 0^\circ$) to make the spacing between transition frequencies wider [see Eq. (6)] and resolve the resonance. However, the two components could not be resolved due to the wide line widths relative to the small eqQ/h. The fitting of a two-component Gaussian was performed, following the same procedure as outlined previously for the analysis of ^{20}Na in ZnO. The setting of crystal angle $\theta = 0^\circ$, which is different form those in ^{20,21}Na measurements, does not introduce systematic errors from the fitting procedure since ZnO has $\eta = 0$

($V_{XX} = V_{YY}$) and therefore the fixed ratio of the electric field gradient in the fitting is same for ^{21}Na and ^{27}Na in ZnO. The centroid of the fit gives the dominant-site eqQ/h of ^{27}Na in ZnO:

$$\left|\frac{eqQ(^{27}\mathrm{Na})}{h}\right|_{\mathrm{ZnO}} = 48 \pm 4 \ \ \mathrm{kHz}. \tag{12}$$

$Q(^{20}\mathrm{Na})$ and $Q(^{21}\mathrm{Na})$ were extracted from Eq. (11), (12) and $Q(^{27}\mathrm{Na})$ [8] as

$$|Q(^{20}\mathrm{Na})| = 10.3 \pm 0.8 \ \ e \ \ \mathrm{fm}^2, \tag{13}$$

$$|Q(^{21}\mathrm{Na})| = 14.0 \pm 1.1 \ \ e \ \ \mathrm{fm}^2. \tag{14}$$

The present result for ^{20}Na is consistent with a previous experiment [31] within the two similar uncertainties. For ^{21}Na, the present result is significantly larger than the previous value [32], with an uncertainty, a factor of three smaller.

The impact of the present results for our understanding of the structure of the neutron-deficient Na isotopes is reported elsewhere [16].

4. SUMMARY

A compact β-NMR/NQR system with a permanent magnet was developed at ISAC/TRIUMF to measure ground-state electromagnetic moments of short-lived nuclides. The system enables application of multiple transition frequencies in a time that is short compared with the lifetime of the nucleus, for efficient NMR measurements in the presence of electric-quadrupole interactions. The β-NMR/NQR technique was applied using highly polarized ^{20,21,26,27,28}Na beams produced by the collinear optical-pumping technique. The degree of nuclear polarization and the T_1s of the Na isotopes in NaF, TiO_2, $LiNbO_3$, MgF_2, ZnO, Pt and Mg single crystals were studied at room temperature. The results are summarized in Table 1. The T_1s in Pt are dominated by the Fermi contact interaction. The T_1s in ionic crystals are inconsistent with the quadrupolar relaxation mechanism, which may be attributed to the roughness of the crystal surfaces. The electric-quadrupole coupling constants of ^{20}Na and ^{21}Na implanted in a ZnO crystal, which maintains polarization well with long T_1s, were measured to be $|eqQ(^{20}\mathrm{Na})/h|_{\mathrm{ZnO}}$ = 690 ± 12 kHz and $|eqQ(^{21}\mathrm{Na})/h|_{\mathrm{ZnO}}$ = 939 ± 14 kHz, respectively. An electric-quadrupole coupling constant of ^{27}Na in ZnO was also measured as $|eqQ(^{27}\mathrm{Na})/h|_{\mathrm{ZnO}}$ = 48 ± 4 kHz. The quadrupole moments of ^{20}Na and

^{21}Na were deduced to be $|Q(^{20}\mathrm{Na})| = 10.3 \pm 0.8$ e fm^2 and $|Q(^{21}\mathrm{Na})| = 14.0 \pm 1.1$ e fm^2, respectively, using the measured $eqQ(^{27}\mathrm{Na})/h$ and the known quadrupole moment of ^{27}Na. The electric-quadrupole coupling constants of ^{20,21}Na in TiO_2 and Mg single crystals are also reported.

ACKNOWLEDGMENT

The authors would like to thank P. F. Mantica at NSCL/MSU for valuable discussions and are grateful to the TRIUMF staff. The study was supported in part by the 21$^{\mathrm{st}}$ century COE program 'Towards a new basic science: depth and synthesis' . One of the authors (K. M. at NSCL/MSU) would like to thank the National Science Foundation for support, Grant PHY06-06007.

[1] K.Matsuta et al., Phys. Lett. B 459 (1999) 81.

[2] G. Neyens et al., Phys. Rev. Lett. 94 (2005) 022501.

[3] G. D. Morris et al., Phys. Rev. Lett. 93 (2004) 157601.

[4] H. -J. Kluge and W. Nörtershäuser, Spectrochimica Acta B 58 (2003) 1031.

[5] E. Arnold et al., Phys. Lett. B 197 (1987) 311.

[6] D. Borremans et al., Phys. Rev. C 72 (2005) 044309.

[7] R. Neugert, Hyperfine Interactions 127 (2000) 101.

[8] M. Keim et al., Eur. Phys. J. A 8 (2000) 31.

[9] C. D. P. Levy et al., AIP Conf. Proc. 980 (2008) 273.

[10] A. Klein et al., Nucl. Phys. A 607 (1996) 1.

[11] C. D. P. Levy et al., Nucl. Instrum. Methods Phys. Res. A 580 (2007) 1571.

[12] K. Asahi et al., Phys. Lett. B 251 (1990) 488.

[13] D. E. Groh et al., Phys. Rev. Lett. 90 (2003) 202502.

[14] G. Neyens, Rep. Prog. Phys. 66 (2003) 633 and 1251.

[15] K. Minamisono et al., Hyperfine Interactions 159 (2005) 261.

[16] K. Minamisono et al., Phys. Lett. B 672 (2009) 120.

[17] C. D. P. Levy et al., Nucl. Phys. A 701 (2002) 253c.

[18] C. D. P. Levy et al., Nucl. Instrum. Methods Phys. Res. B 204 (2003) 689.

[19] A group of codes, POISSON/SUPERFISH, http://laacg1.lanl.gov/laacg/services/download_sf.phtml.

[20] A. Abragam, *The Principles of Nuclear Magnetism*, (Oxford University Press, Oxford, 1986) p. 232.

[21] A. Abragam, *The Principles of Nuclear Magnetism*, (Oxford University Press, Oxford, 1986) p. 65.

[22] T. Minamisono et al., Hyperfine Interactions 80 (1993) 1315.

[23] K. Minamisono et al., Nucl. Instrum. Methods Phys. Res. A 589 (2008) 185.

[24] N. J. Stone, At. Data Nucl. Data Tables 90 (2005) 75.

[25] R. V. Pound, Phys. Rev. 79 (1950) 685.

[26] R. L. Mieher, Phys. Rev. Lett. 4 (1960) 57.

[27] A. Abragam, *The Principles of Nuclear Magnetism*, (Oxford University Press, Oxford, 1986) p. 354.

[28] T. Minamisono et al., Phys. Lett. B 420 (1998) 31.

[29] R. E. J. Sears, J. Chem. Phys. 66 (1977) 5250.

[30] H. Schweickert et al., Nucl. Phys. A 246 (1975) 187.

[31] M. Keim, AIP Conf. Proc. 455 (2000) 50.

[32] F. Touchard et al., Phys. Rev. C 25 (1982) 2756.

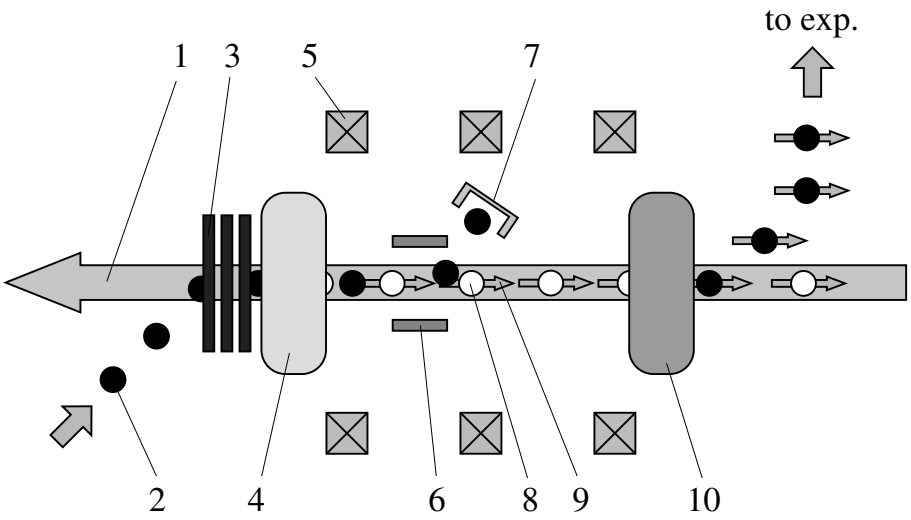

Figure 1: Schematic illustration of polarizer beam line at ISAC-I. The numbers indicate 1: circularly polarized laser light, 2: singly charged ion beam, 3: Doppler tuning electrodes, 4: Na-vapor neutralizer cell, 5: coils providing the weak-magnetic guiding field, 6: ion deflector, 7: Faraday cup, 8: neutral atom, 9: polarization and 10: He gas re-ionizer cell.

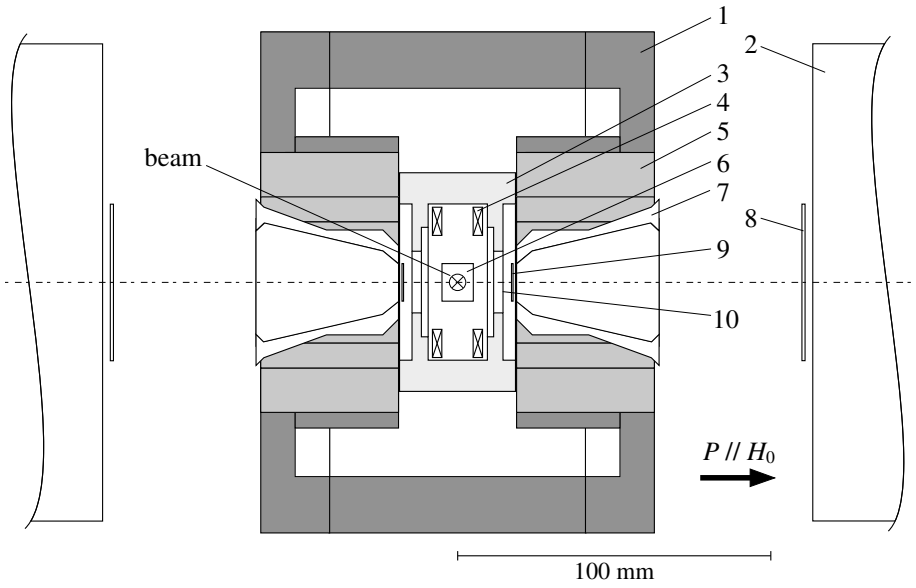

Figure 2: Cross section of the β-NMR system. The system (with the exception of the RF coils) is axially symmetric around the horizontal central line (the dot-dashed line). The numbers indicate 1: return yoke (iron), 2: counter E, 3: vacuum chamber (plastic), 4: RF coils, 5: permanent magnet, 6: implantation crystal, 7: counter C, 8: counter B, 9: counter A, and 10: plastic β window. The polarized beam was incident perpendicular to the plane of the paper. The magnetic field was applied parallel to the direction of polarization, which is indicated by an arrow. The RF field was applied perpendicular to H_0.

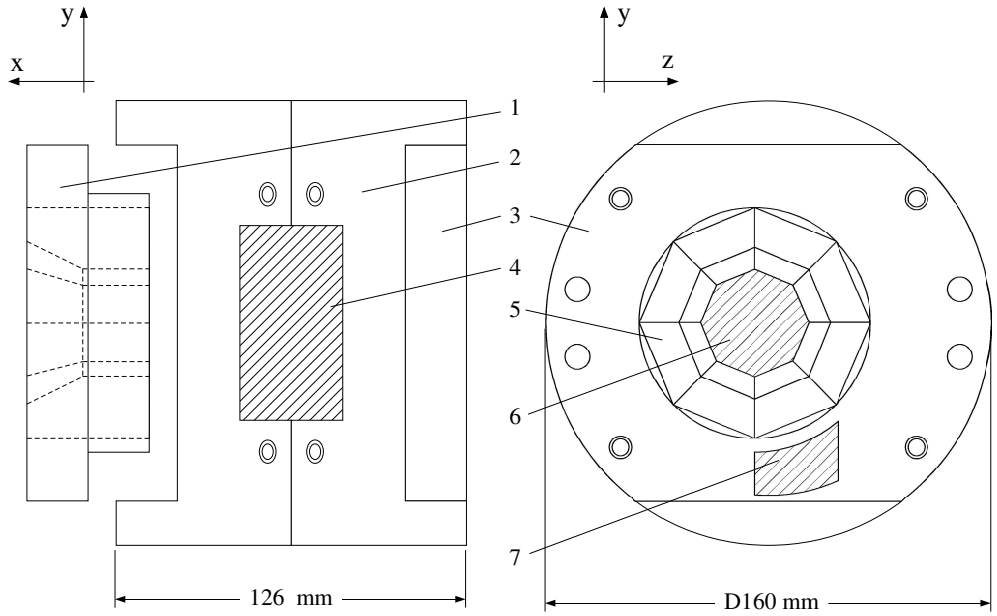

Figure 3: The NMR magnet. The beam and vertical directions are taken to be z and y directions, respectively. One of the poles is removed from the return yoke to illustrate how it was assembled. The numbers indicate 1 and 3: permanent-magnet poles, 2: return yoke (iron), 4: opening for vacuum chamber (not drawn), 5: permanent magnet, 6: opening for counter C (not drawn) and 7: opening for counter A (not drawn).

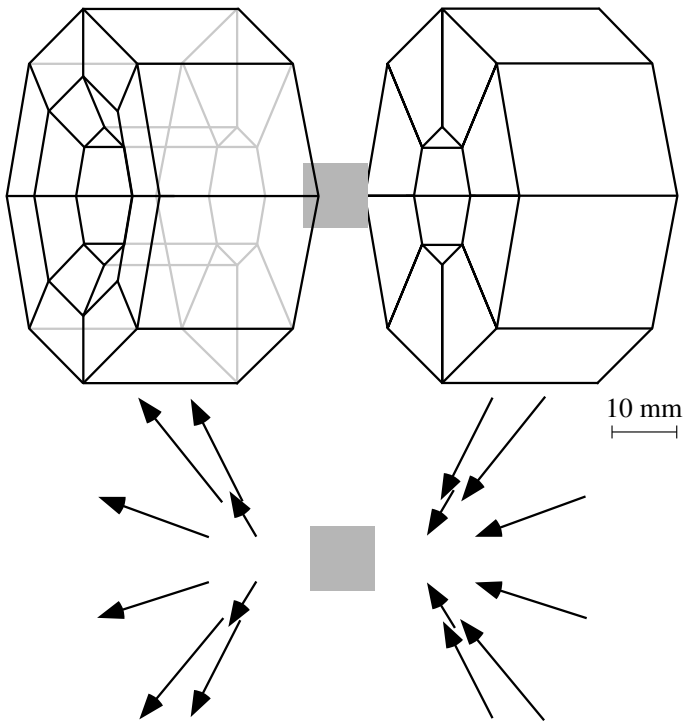

Figure 4: The permanent magnets. Each pole of the magnet consisted of 8 segments. The field directions were adjusted, as shown in the lower part of the figure, for good uniformity of the field at the center of the magnet. The catcher crystal is shown by the gray square.

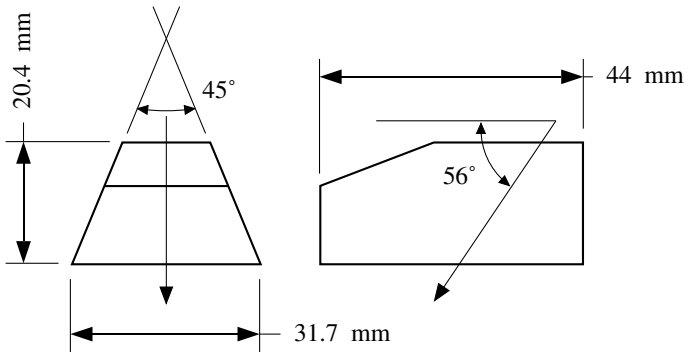

Figure 5: One segment of the permanent magnet. The arrows indicate directions of magnetization axis. One permanent-magnet pole consisted of eight segments.

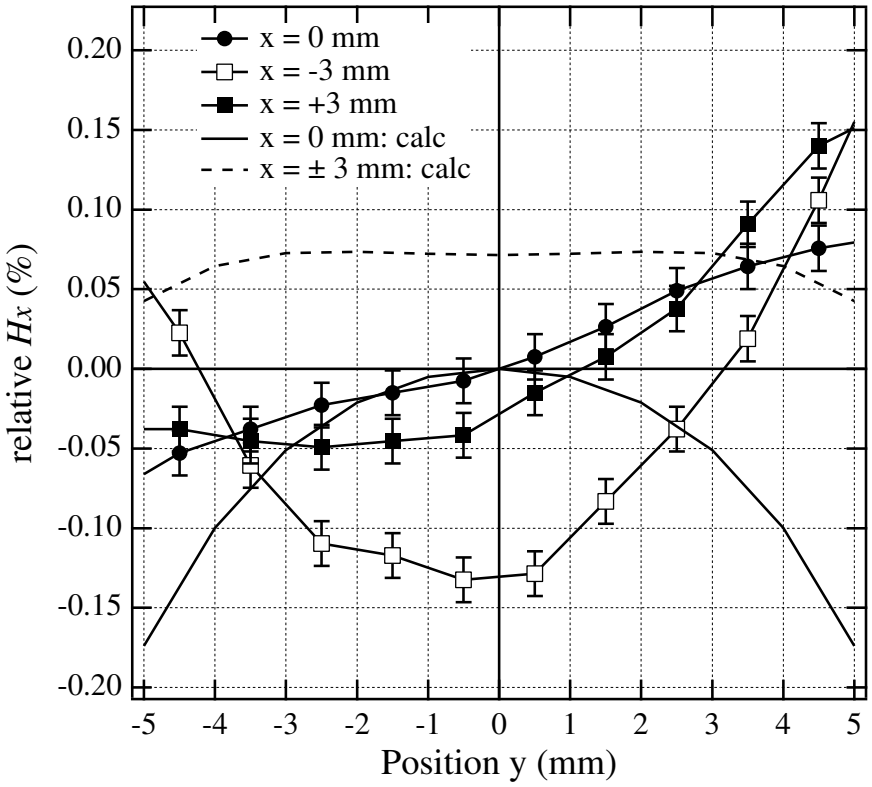

Figure 6: Magnetic field distribution of the NMR magnet. The same coordinate system as used in Fig. 3 is used, and the origin is the center of the magnet. Data points are the measurements by a Hall probe and lines are to guide the eye. The solid and dashed lines are results of calculations by PANDIRA at x = 0 and ±3 mm, respectively. A cylindrical symmetry around x axis was assumed in the calculation. The strength of the magnetic field in the x direction was measured along the y direction, for three different x positions. Results are plotted relative to the central field of strength $H_0 = 0.5286$ T. The results of calculations are plotted relative to the calculated value at the center. Vertical bars of the data points represent precision of measurements. The absolute H field value, however, may deviate by ± 0.5% from the true value, due to a calibration of the Hall probe. The catcher was in the x-y plane at z = 0 mm and typical beam size was about 5 mm in diameter. The asymmetric distributions around the x and y axes are attributed to the accuracy in setting the magnetization axes at 56°.

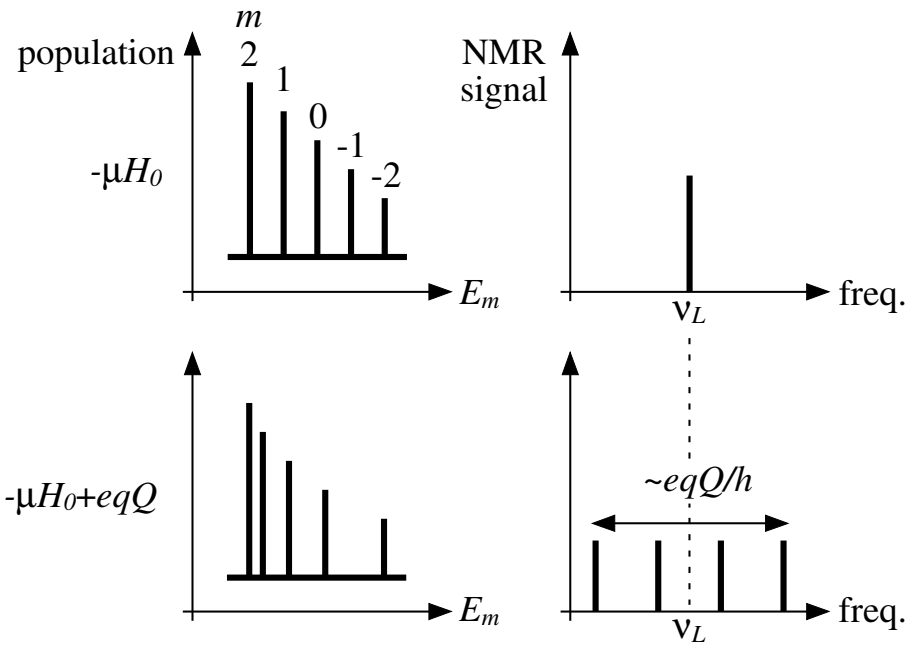

Figure 7: Energy levels and transition frequencies for an $I = 2$ nucleus. In the upper panel, energy levels are shown in the presence of a purely magnetic-dipole interaction. A single resonance frequency (ν_L, the Larmor frequency) results, due to the evenly spaced energy levels. When the electric-quadrupole interaction is added, as shown in the lower panel, the spacings between adjacent substates become uneven and $2I$ different resonance frequencies result.

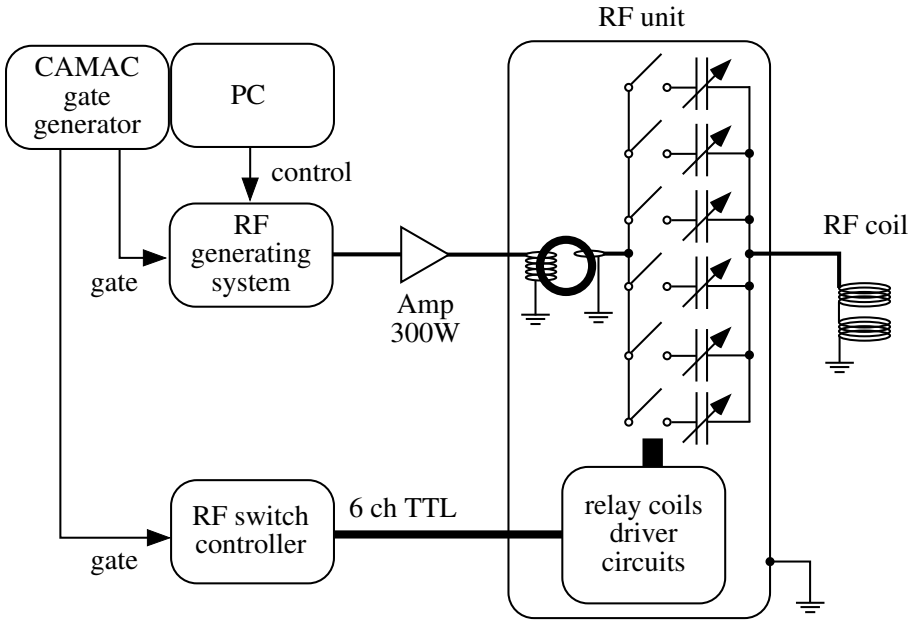

Figure 8: Schematic illustration of the β-NQR RF system. The RF coil is in a vacuum chamber, which is not drawn here. The bold circle in the RF unit is a ferrite core for the impedance matching.

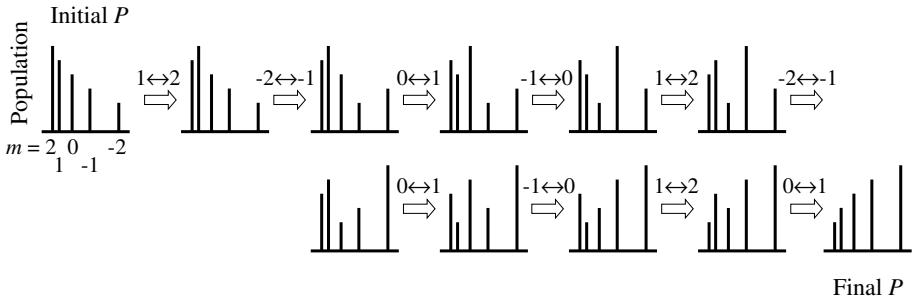

Figure 9: Schematic illustration of the inversion of initial polarization by AFP for an $I = 2$ nucleus such as ^{20}Na. $1 \leftrightarrow 2$, for example, indicates an application of the transition frequency between $m = 1$ and 2 magnetic substates and the populations in these two substates are interchanged by the AFP. Note that the spacings among energy levels are uneven due to the electric-quadrupole interaction.

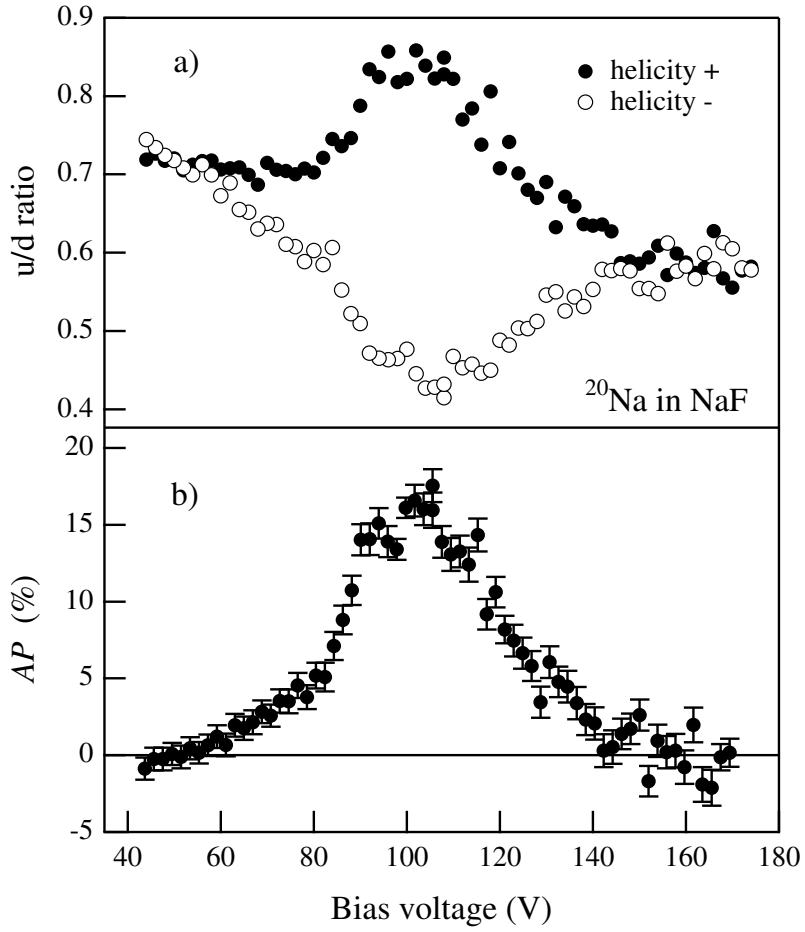

Figure 10: Results of bias scans for ^{20}Na in NaF. a): the u/d β-ray counting ratios with positive- (solid circles) and negative- (open circles) helicity laser light. b): the deduced AP as a function of Na cell bias voltage.

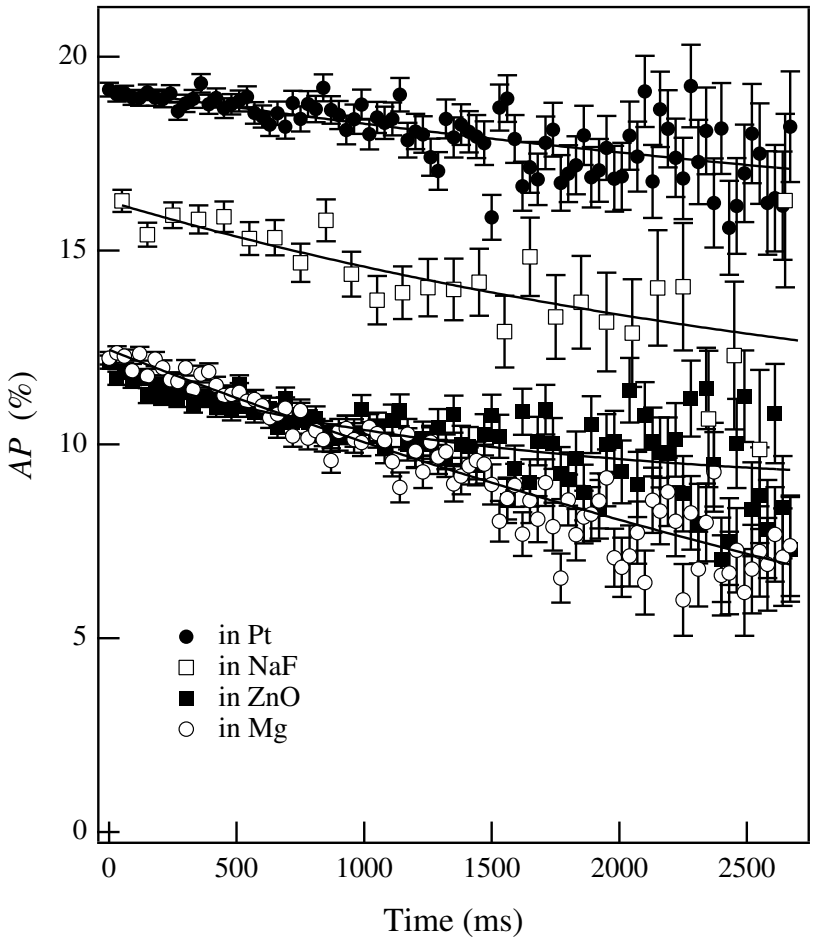

Figure 11: Spin-lattice relaxation times of ^{20}Na in various single crystals. The variation of AP is plotted as a function of time. The symbols are data and the solid lines are exponential fits to the data.

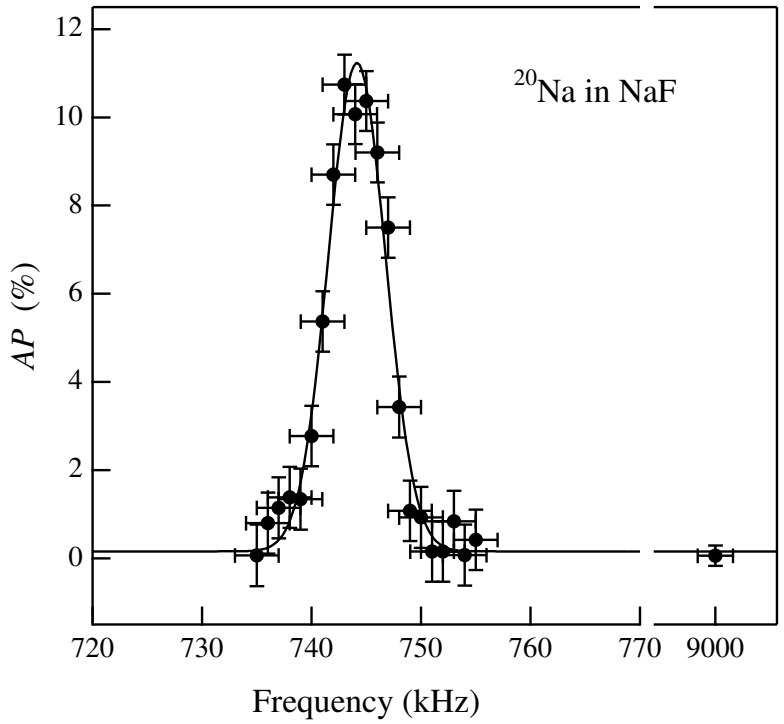

Figure 12: The NMR spectrum of ^{20}Na in a NaF single crystal (cubic). The solid circles are data and the horizontal bar for each point represents the applied FM. The solid line is a Gaussian fit to the data. A depolarization method was used to precisely determine the ν_L.

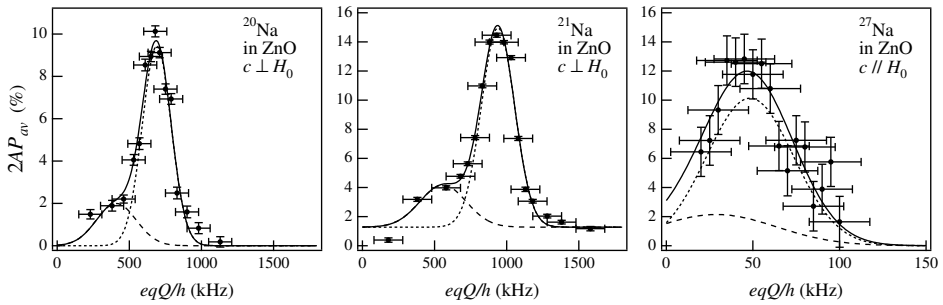

Figure 13: NQR spectra of ^{20}Na, ^{21}Na and ^{27}Na in a ZnO single crystal. The solid circles are data and the horizontal bar for each point is the range in eqQ/h probed by the FM. The solid line is a two-Gaussian fit to the data with two components shown by a dotted line and a broken line.

Table 1: Measured asymmetry change, relaxation time and extracted initial polarization of Na isotopes implanted in single crystals. All measurements were performed at room temperature. See the text for notations.

	^{20}Na	^{21}Na	^{26}Na	^{27}Na	^{28}Na
$T_{1/2}$	447.9 (ms)	22.49 (s)	1.072 (s)	301 (ms)	30.5 (ms)
I^{π}	2^+	$3/2^+$	3^+	$5/2^+$	1^+
A	+0.33	+0.81	-0.94	-0.88	-0.76
$\mu(\mu_N)$ [24]	+0.3694(2)	+2.3861(1)	+2.851(2)	+3.895(5)	+2.426(3)
Q (e fm^2)	10.3 ± 0.8 [16]	14.0 ± 1.1 [16]	-0.53 ± 0.02 [8]	-0.72 ± 0.03 [8]	+3.95 ± 0.12 [8]
			NaF(cubic)		
AP (%)	16.0 ± 0.4	20.8 ± 0.2	-46.6 ± 1.1	-37.1 ± 1.9	-35.9 ± 2.5
T_1 (s)	9.9 ± 3.1	9.0 ± 0.2	24.6 ± 4.2	8.1 ± 1.8	-
P_0 (%)	51.0 ± 1.3	33.5 ± 0.5	52.8 ± 1.3	45.3 ± 2.4	-
			TiO_2(rutile)		
AP (%)	5.3 ± 0.3	13.7 ± 0.3	-44.8 ± 0.5	-42.9 ± 1.0	-34.1 ± 2.5
T_1 (s)	3.4 ± 1.3	13.0 ± 0.5	32 ± 11	13.5 ± 2.6	-
P_0 (%)	18.3 ± 1.5	24.0 ± 0.5	46.8 ± 0.9	50.9 ± 1.2	-
$\lvert eqQ/h\rvert$ (MHz)	-	5.20 ± 0.03	-	-	-
η		0.33 ± 0.03	-	-	-
			$LiNbO_3$(illmenite)		
AP (%)	4.3 ± 0.3	5.3 ± 1.6	-40.4 ± 0.6	-	-26.3 ± 3.0
T_1 (s)	1.8 ± 0.5	1.3 ± 0.3	5.3 ± 0.5	-	-
P_0 (%)	17.0 ± 1.7	56 ± 28	51.8 ± 1.5	-	-
			MgF_2(rutile)		
AP (%)	3.0 ± 0.6	-	-18.6 ± 0.6	-	-
T_1 (s)	5.9 ± 0.2	-	7.4 ± 2.0	-	-
P_0 (%)	10.0 ± 2.1	-	22.3 ± 1.3	-	-
			ZnO(hcp)		
AP (%)	11.2 ± 0.3	19.7 ± 0.3	-	-33.0 ± 2.0	-
T_1 (s)	9.0 ± 0.5	9.63 ± 0.09	-	9.5 ± 2.5	-
P_0 (%)	37 ± 1	29.7 ± 0.4	-	39.9 ± 2.5	-
$\lvert eqQ/h\rvert$ (kHz)	690 ± 12	939 ± 14	-	48 ± 4	-
			Pt(fcc)		
AP (%)	18.3 ± 0.3	-	-14.5 ± 0.4	-	-
T_1 (s)	22.0 ± 1.9	-	0.78 ± 0.08	-	-
P_0 (%)	57.0 ± 1.1	-	55.0 ± 5.9	-	-
			Mg(hcp)		
AP (%)	11.0 ± 0.2	-	-	-	-
T_1 (s)	4.5 ± 0.1	-	-	-	-
P_0 (%)	39.3 ± 0.8	-	-	-	-
$\lvert eqQ/h\rvert$ (kHz)	36.7 ± 0.7	-	-	-	-